Correction of walk-off-induced wavefront distortion for continuous-wave laser*

Hongxin Zou(邹宏新)†, Guozhu Chen(陈国柱), Yue Wu(伍越), Yong Shen(沈咏), and Qu Liu(刘曲)

Department of Physics, The National University of Defense Technology, Changsha 410073, *China*

(Received 2 February 2016; published online 2 August 2016)

We theoretically and experimentally investigate the wave front distortion in critically phase-matched continuous-wave (CW) second harmonic generation (SHG). Due to the walk-off effect in the nonlinear crystal, the generated second harmonic is extremely elliptical and quite non-Gaussian, which causes a very low matching and coupling efficiency in experiment. Cylindrical lenses and walk-off compensating crystals are adopted to correct distorted wave fronts, and obtain a good TEM_{00} mode efficiently. Theoretically, we simulate the correction effect of 266-nm laser generated with SHG. The experiment results accord well with the theoretical simulation and an above 80% TEM_{00} component is obtained for 266-nm continuous-wave laser with a 4.8°-walk-off angle in beta barium borate (BBO) crystal.

Keywords: optical nonlinearity, walk-off effect, wavefront distortion

PACS: 42.60.By, 42.65.Ky, 42.72.Bj **DOI:** 10.1088/1674-1056/25/9/094211

1. Introduction

The innovation in material science, chemistry, communications, and many other fields has stimulated an increasing interest in ultraviolet (UV) coherent radiation. Considering that the available wavelength range of conventional lasers is usually limited, nonlinear frequency transformation is a commonly adopted solution in generating UV lasers.[1] Most of nonlinear materials have a strong absorption for light with a wavelength less than 300 nm, which are not suitable for UV radiation generation. Borate crystals, such as beta barium borate (BBO), cesium lithium borate (CLBO), and potassium fluoro–beryllo–borate (KBBF), have excellent transmittance as well as good nonlinearity in this spectrum range, and is thus the only available option nowadays.[2–4] In critical phase matching, beams unavoidably suffer from the walk-off effect, which significantly decreases the overlap and interaction between different beams and degrades the conversion efficiency. Plenty of effort has been devoted to fighting against the walk-off effect. Steinbach *et al.* have proposed using elliptical fundamental beams to increase the beam overlap and hence promote the conversion efficiency.[5] Walk-off compensating crystals are also adopted to further suppress the walk-off effect and promote the conversion efficiency.[6–9] In those studies, only the output power and conversion efficiency are concerned. However, in a continuous-variable regime,[10,11] the phase distortion of the beam must be properly dealt with. Because one needs to interfere the signal beam with a reference to perform a measurement on two quadratures of the field, and the mode mismatching will compromise the detection efficiency.

In this paper, we theoretically and experimentally investigate the intensity and phase distortion of the output wavefront from the type I critically phase-matched continuous-wave second harmonic generation in a BBO crystal. We use a heuristic method developed by Boyd and Kleinman[12] to obtain the numerical simulation result, and compared it with that measured using an interferometer experimentally. The result shows that even though the generated second harmonic can be reshaped circular with cylindrical lenses, the phase distribution is still distorted, which leads to a relatively small proportion of the TEM_{00} mode component. In order to obtain the TEM_{00} mode more efficiently, we replace the normal single bulk BBO crystal with an optically contacted walk-off compensating configuration. With both numerical simulation and experimental demonstration, we verify that this configuration can improve wave front distortion and obtain a higher proportion of the TEM_{00} mode component correspondingly.

2. Theoretical simulation

In optical communication and metrology, continuous-wave coherent radiation in a large part of the spectrum range is desired. To generate ultraviolet laser beams, cavity enhanced SHG is usually employed. In this paper, we will mainly concentrate on the type I critically phase-matched SHG.

2.1. Beam distortion induced by walk-off effect

In SHG, the electric field of the fundamental beam can be expressed by the q parameter as

$$E(x,y,z) = \frac{A_1}{\sqrt{(q_x+z)(q_y+z)}}$$

*Project supported by the National Natural Science Foundation of China (Grant No. 91436103) and Research Programme of National University of Defense Technology, China (Grant No. JC15-02-03).

†Corresponding author. E-mail: hxzou@nudt.edu.cn

© 2016 Chinese Physical Society and IOP Publishing Ltd

$$\times \exp\left\{-\mathrm{i}k_1\left[z+\frac{x^2+y^2}{2\sqrt{(q_x+z)(q_y+z)}}\right]\right\}, \quad (1)$$

where A_1 is the amplitude, $q_{x,y}=\mathrm{i}\pi\omega_{1x,y}/\lambda_1+z_{0x,y}$ is the q parameter, $\omega_{1x,y}$ is the beam waist size along the x and y axes, $z_{0x,y}$ is the waist position, λ_1 is the wavelength of the beam, and k_1 is the wave vector.

For continuous-wave operation, the peak intensity is much lower than that of a pulse laser normally, thus the conversion efficiency is also much lower, which means that the depletion induced by up conversion can be ignored. Under this scenario, we do not need to solve the complicated field evolution equations, only a simple heuristic method developed by Boyd and Kleinman[12] would suffice. Results obtained with this approximate method are in excellent accordance with the exact yet tedious numerical solution.[13] In this model, the nonlinear medium is divided into many slices, while the second harmonic fields with extraordinary polarization are generated at each slice by the local fundamental field and then propagate independently and interfere in the end with each other to compose the final output field. If the nonlinear medium is a single bulk crystal, the second harmonic generated before and after the fundamental beam waist will have the same walk-off angle and propagate to different positions, as shown in Fig. 1. For a single bulk crystal, the electric field of the generated second harmonic can be expressed as[12]

$$\begin{aligned}&E_1(x,y,z)\\&=\int_{-l/2}^{l/2}\mathrm{d}z' f(z,z')\\&\quad\times\exp\left\{-\mathrm{i}k_2\left[z+\frac{x^2+(y-\rho(l/2-z'))^2}{2\sqrt{(q_{1x}+z)(q_{1y}+z)}}\right]\right\},\end{aligned} \quad (2)$$

where $f(z,z')=A_1^2/\sqrt{(q_{1x}+z')(q_{1y}+z')(q_{1x}+z)(q_{1y}+z)}$, ρ is the walk-off angle, l is the length of the nonlinear crystal. Here, we have assumed that ρ is small, and the waist of the fundamental beam is located at the center of the crystal. In this formula, the field generated at each slice is still described by a Gaussian beam with the same q parameter. With this equation, we can obtain the intensity $I=|E|^2$ and phase $\varphi=\mathrm{Arg}E$ of the generated second harmonic.

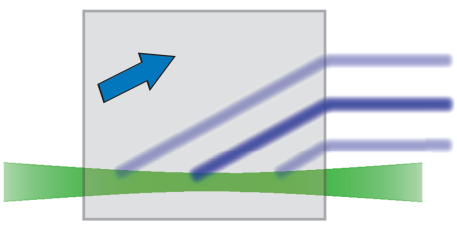


Fig. 1. (color online) Illustration of the second harmonic generation in the BBO crystal with a single bulk configuration. The arrow indicates the direction of the extraordinary principle axis.

In our previous work, we built an SHG cavity containing a 7-mm BBO crystal to generate 266-nm laser.[14] The walk-off angle in our case is 83.77 mrad. It is shown that the generated beam is extremely elliptical at the far field, and can be reshaped to be almost circular if we put a cylindrical lens at a proper position and focus the noncritical direction.[15] At a plane 4-m behind the center of the crystal, the intensity and phase distributions of the beam along the x direction are still Gaussian, which are not surprising, since no walk off occurs in this direction. Thus, we do not bother to plot them here. The intensity distribution of the reshaped beam along the y direction also looks Gaussian, as shown in Fig. 2. However, things are quite different when it comes to the phase distribution. Although we have focused the fundamental beam to the center of the nonlinear crystal, the generated second harmonic is still quite asymmetric. As shown in Fig. 2, the center of the phase distribution has a significant shift relative to the center of the intensity distribution, which implies that this beam is quite non-Gaussian and has a lot of higher-order mode components.

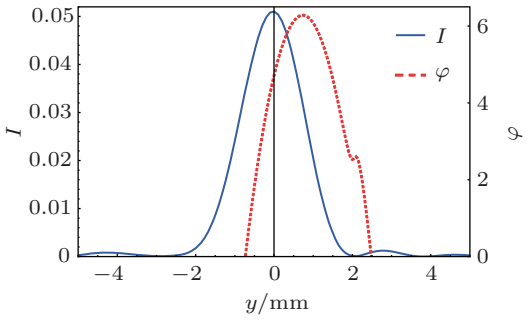


Fig. 2. (color online) Intensity (solid line) and phase (dashed line) distributions of the generated second harmonic along the y axis with a single bulk BBO crystal.

2.2. Distortion correction with compensating crystals

To suppress the walk-off effect, the compensating crystal configuration has been adopted, and the conversion efficiency can be promoted.[6–9] In this configuration, the nonlinear medium is separated into two identical crystals, whose opposite crystal axes are symmetrically oriented relative to the beam propagation direction, as shown in Fig. 3. To suppress the walk-off effect most efficiently, the beam waist of the fundamental beam should be focused to the interface of these two crystals. We find that this configuration also helps to alleviate beam distortion. In this case, to simulate the generated electric field, we can still use the formula introduced above, only if we separate the integral into two parts, with opposite walk-off angles. Thus the electric field of the generated second harmonic can be written as

$$\begin{aligned}&E_2(x,y,z)\\&=\int_{-l/2}^{0}\mathrm{d}z' f(z,z')\end{aligned}$$

$$\times \exp\left\{-\mathrm{i}k_2\left[z+\frac{x^2+(y-\rho(l/2+z'))^2}{2\sqrt{(q_{1x}+z)(q_{1y}+z)}}\right]\right\}$$
$$+\int_0^{l/2}\mathrm{d}z' f(z,z')$$
$$\times \exp\left\{-\mathrm{i}k_2\left[z+\frac{x^2+(y-\rho(l/2-z'))^2}{2\sqrt{(q_{1x}+z)(q_{1y}+z)}}\right]\right\}. \quad (3)$$

In this configuration, the intensity and phase distributions of the generated second harmonic at the far field are plotted according to Eq. (3), as shown in Fig. 4. From this figure, we can see that in this case the asymmetry of the phase distribution in the y axis is much more subtle than that when a single bulk crystal is used, which implies that the beam distortion is greatly reduced.

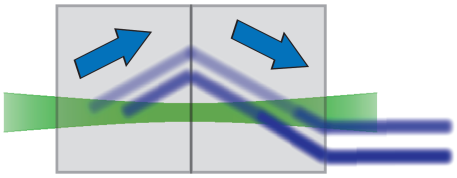


Fig. 3. (color online) Illustration of second harmonic generation in the BBO crystal with two-crystal compensating configuration. The arrows indicate the direction of the extraordinary principle axes of the crystals.

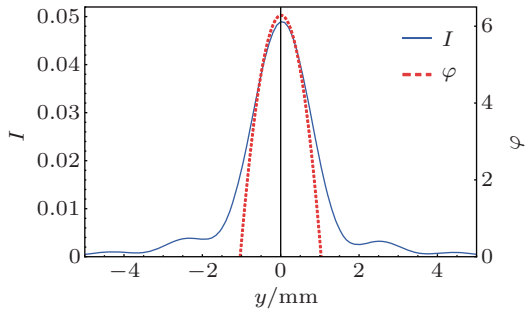


Fig. 4. (color online) Intensity (solid line) and phase (dashed line) distributions of the generated second harmonic along the y axis with two-crystal compensating configuration.

This method can be generalized to configurations with more identical crystals, where the optical axes of the crystals are flipped in sequence. To optimize the conversion efficiency, the waist of the fundamental beam should still be focused to the center of the series of crystals. For a configuration with n crystals ($n \geq 2$), the electric field of the generated second harmonic can be expressed as

$$E_n(x,y,z)$$
$$= \sum_{i=0}^{\lfloor\frac{n-1}{2}\rfloor}\int_{\frac{(n/2-1-2i)l}{n}}^{\frac{(n/2-2i)l}{n}}\mathrm{d}z' f(z,z')$$
$$\times \exp\left\{-\mathrm{i}k_2\left[z+\frac{x^2+(y-\rho(\frac{(n/2-2i)l}{n}-z')^2}{2\sqrt{(q_{1x}+z)(q_{1y}+z)}}\right]\right\}$$
$$+\sum_{i=1}^{\lfloor\frac{n}{2}\rfloor}\int_{\frac{(n/2-2i)l}{n}}^{\frac{(n/2+1-2i)l}{n}}\mathrm{d}z' f(z,z')$$
$$\times \exp\left\{-\mathrm{i}k_2\left[z+\frac{x^2+(y-\rho(z'-\frac{(n/2-2i)l}{n}))^2}{2\sqrt{(q_{1x}+z)(q_{1y}+z)}}\right]\right\}, \quad (4)$$

where $\lfloor x \rfloor$ is the floor of x. Naively, we may expect that with more compensating crystals, the walk-off effect would be more strongly suppressed. However, with numerical simulation we find that it is not true, as we will discuss in the following.

2.3. Transverse mode properties of corrected beams

To quantitatively assess the performance of the distortion correction scheme, we need to analyze the spatial properties of the generated distorted second harmonic mode, which can be carried out by expanding it with a proper set of Hermite-Gaussian modes. The electric field of Hermite–Gaussian modes can be written as

$$E_n(x,z) = A\left(\frac{q_0}{q(z)}\right)^{1/2}\left[\frac{q_0 q^*(z)}{q^* q(z)}\right]^{n/2}\mathrm{H}_n\left(\frac{\sqrt{2}x}{\omega(z)}\right)$$
$$\times \exp\left[-\mathrm{i}\frac{kx^2}{2q(z)}\right]. \quad (5)$$

Since it is the TEM_{00} that is usually of interest in experiments, we wish to extract the TEM_{00} mode from the distorted mode as much as possible. Thus, among all sets of Hermite–Gaussian (HG) modes, we need to find the one in which the TEM_{00} mode has the maximum overlap with the distorted mode. This can be done by scanning the waist size ω and position z_0 of a TEM_{00} mode. Since there is no walk off in the x direction, all the Gaussian properties are preserved in this direction. Thus we only need to consider the y direction. Once these parameters are determined, the distorted mode can be expanded with a proper set of HG modes.

With the proper set of Hermite–Gaussian modes, we obtained the proportion of transverse mode components for the generated second harmonic with configurations using one, two, three, and four crystals, as shown in Fig. 5. Since there is no walk off along the x axis, the Gaussian distribution preserves along this direction, thus only TEM_{0n} mode components are presented. We found that, for a single bulk crystal, the maximum overlap of only about 70.3% can be achieved. Due to the significant walk off induced phase asymmetry along the y axis, large TEM_{01} mode components exhibit in the distorted second harmonic, which makes it quite difficult to be mode matched in homodyne detection.

The TEM_{00} mode has a better overlap when two compensating crystals are applied. The simulation result shows that the maximum overlap can reach 89.0%, which is much higher than that for a single bulk crystal. The large TEM_{01} mode in the previous configuration now almost vanishes. There is only a tiny peak for the TEM_{03} mode due to the residual intensity asymmetry in the wavefront. Here, it should be noticed that

there are also other higher-order mode components for both configurations. However, their proportions are too small to be visible in this figure.

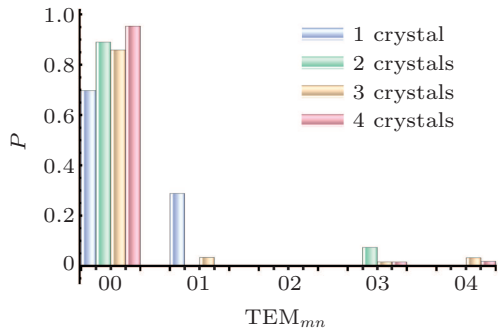


Fig. 5. (color online) Proportion of TEM$_{mn}$ mode components of the distorted second harmonic generated by one, two, three, and four crystals, respectively.

However, if three crystals are adopted, the proportion of TEM$_{03}$ mode component of the generated second harmonic becomes lower than that with just two crystals, as shown in Fig. 5. The TEM$_{03}$ mode component emerges again, which implies that the decrease of the symmetry of the wavefront. However, it is still higher than that generated by one crystal. For four crystals, things are different again. When four crystals are applied, the generated beam has more TEM$_{00}$ mode components than the configuration with two crystals, as shown in Fig. 5. Only a little high-order mode components exhibit due to the residual asymmetry of the wavefront.

2.4. Analysis of the distortion correction scheme

The mechanism of the distortion correction scheme can be concluded into two points. The first is obvious and straightforward. Due to the walk-off effect, the generated second harmonics at each slice of the crystal will be separated in space. For an n-crystal configuration, the maximum separation d_n is related to the length of each crystal and can be written as

$$d_n = \tan\rho\frac{l}{n} \approx \rho l/n, \tag{6}$$

where l is the total length of all the crystals. With more crystals, the separation of all the generated second harmonics will be less, which means that the beams are more concentrated and can interfere more constructively.

The second is related to the Gouy phase. For a single bulk crystal, according to Eq. (2), due to the second-order nonlinear effect, the generated second harmonic in a slice of the crystal at z' will carry an extra complex coefficient $c_1(z')$ induced by the Gouy phase of the fundamental beam, which can be written as

$$c_1(z') = \frac{1}{\sqrt{(q_{1x}+z')(q_{1y}+z')}}. \tag{7}$$

Generally, the phase of $c_1(z')$ is related to z'. Due to the additional phase, the generated beams will interfere more destructively. Thus, the second harmonic becomes quite asymmetric at the far field. This effect becomes more prominent if the fundamental beam is focused tighter. Unlike the pulsed laser, whose peak intensity is already quite high, the continuous-wave field is usually more tightly focused to make the intensity high enough in nonlinear processes, so as to ensure a decent conversion efficiency. Therefore, there is more significant wave front distortion in continuous-wave operation than in pulsed laser operation.

However, for two-crystal compensating configuration, as shown in Fig. 3, since the two crystals have opposite walk-off directions, the second harmonic generated at slices symmetric with the interface will perfectly overlap with each other. Thus, the second harmonic is more concentrated in this case. Moreover, for a pair of slices, the complex coefficient can be written as

$$c_2(z') = \frac{1}{\sqrt{(q_{1x}+z')(q_{1y}+z')}} + \frac{1}{\sqrt{(q_{1x}-z')(q_{1y}-z')}}, \tag{8}$$

where $z' > 0$ is the distance from each slice to the interface of the two crystals. Since $q_{1x,1y}$ is imaginary and z' is real, with straightforward derivation, we find that $c(z')$ is real, that is, the phase of $c_2(z')$ is independent of z', which implies that the second harmonic generated by every pair of slices carries the same Gouy phase. Therefore, all the generated second harmonics are more coherent and can interfere more constructively with each other.

It also explains why even n-crystal configurations show better performance than odd n configurations. Since for even n, the coefficient $c_n z'$ always has paired terms with opposite imaginary parts, which gives rise to a real $c_n z'$, whose phase is independent of z'. Thus the beam can interfere more constructively. While for odd n, there will always be an unpaired term in $c_n z'$, which leads to a z' dependent Gouy phase. Thus the beam will interfere more destructively.

This can be further justified by checking the wavefront evolution with propagation. According to Eqs. (2) and (3), we plot the beam cross sections at $z = l/2$, $3l$, $10l$, and $1000l$ for configurations with a single bulk crystal and two compensating crystals, as shown in Fig. 6. We can see that at the end of the crystal where $z = l/2$, the beam generated by a single bulk crystal is more spread, while for two compensating crystals the generated beam is more concentrated. As the beams propagate, the former interferes more destructively, while the latter interferes more constructively. That explains why at the far field, for example at $z = 1000l$, even though the intensity distributions of the two beams look almost the same, the phase distributions are prominently distinct from one another.

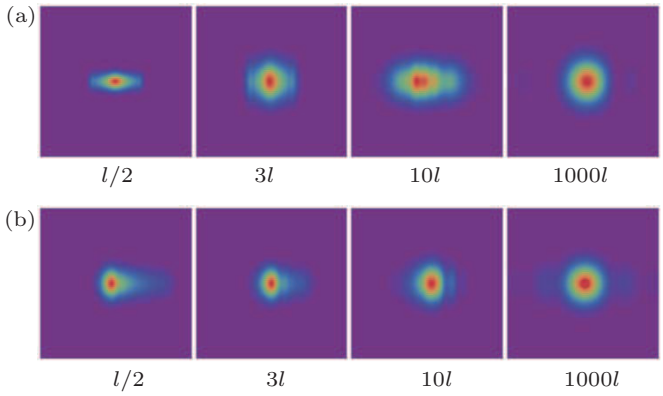


Fig. 6. (color online) Beam cross sections of the generated second harmonic generated by (a) a single bulk crystal and (b) two compensating crystals at $z = l/2$, $3l$, $10l$, and $1000l$.

3. Experimental demonstration

3.1. Experiment setups

To verify the numerical simulation, we generated the distorted second harmonic and built an interferometer to analyze the phase distribution experimentally. The experimental schematic is shown in Fig. 7. The 532-nm fundamental field is phase modulated by an electric optical modulator (EOM) and then resonantly enhanced by a bow-tie cavity with PDH locking. A BBO crystal is placed at exactly the waist of the cavity mode, which is AR coated for both the fundamental and second harmonic fields. To achieve phase matching between 532-nm and 266-nm radiation in BBO, type I critical phase matching is employed. In this configuration, the polarization of the fundamental beam is along the ordinary principle axis, while the second harmonic oscillates along an extraordinary axis and thus walks off in the y axis with an angle of 83.77 mrad. The R2 is a dichroic concave mirror which is HR coated for the 532-nm beam and AR coated for the 266-nm beam.

For 1-W fundamental pump power, the finesse of the cavity is measured to be 160. To further enhance the conversion efficiency, an elliptical cavity mode is adopted,[14] with waists of 12 μm and 26 μm in x and y axes, respectively. When the single bulk crystal is replaced by the walk-off compensating crystals, the finesse of the SHG cavity drops to 143, which shows that the extra loss induced by the interface is about 0.5% for the fundamental beam. As for the second harmonic, it is reasonable to estimate that the loss is of the same order. The output second harmonic is focused by a cylindrical lens L2 along the x axis, the noncritical direction, so as to be reshaped nearly circular at the far field.

To analyze the phase distribution of the distorted beam, we send it to an interferometer to interfere with a local oscillator (LO). As a phase reference, this beam should be coherent with the distorted beam and have an identical phase at each point of the wavefront. To generate it, we split a part of the output beam from the SHG cavity and use a triangle ring cavity as a mode cleaner to purify it. Mirrors of the mode cleaner are well chosen so that impedance matching can almost be achieved. In the interferometer, we use a 1-Hz ramp wave to scan the piezo mirror in the reference path, and record the interference patten using a high speed CCD camera with an acquisition rate of 25 Hz. The intensity at a pixel can be written as

$$I(x,y,t) = E_s^2(x,y) + E_L^2(x,y) + 2E_s(x,y)E_L(x,y) \times \cos[vt/\lambda + \theta(x,y)], \quad (9)$$

where x and y are coordinates of the pixel, E_s and E_L are the amplitudes of the distorted beam and the LO at the pixel, respectively, v is the scanning speed of the piezo mirror, λ is the wavelength, and θ is the relative phase of the distorted beam at the pixel. Since the LO is well collimated, its phase can be taken as a constant at the plane of the CCD camera. By fitting the intensity evolution of each pixel with a sinusoidal function, we can obtain the relative phase of the distorted beam at each pixel. Thus, the phase distribution of the distorted wavefront can be reconstructed.

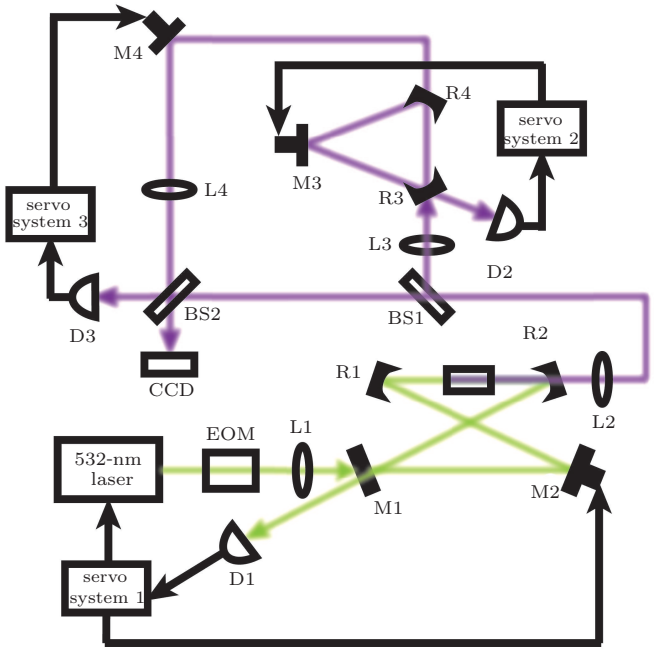


Fig. 7. (color online) Experimental schematic for measuring the phase distribution of the distorted wavefront of the generated second harmonic. EOM: electric optical modulator; L1–L4: lenses; M1–M4: mirrors; R1–R4: concave mirrors; D1–D3: detectors; BS1 and BS2: beamsplitters.

3.2. Results and discussion

By scanning the piezo mirror M3, we obtained the transmission spectrum of the distorted second harmonic, as shown in Fig. 8(a). We can see that the proportion of the demanded TEM_{00} mode only reaches 61%, while about 27% of the power goes into the TEM_{01} mode due to the phase asymmetry. Some higher-order modes are also presented due to slight aberration

and astigmatism. The transmission spectrum from the triangle ring cavity with walk-off compensated crystals is shown in Fig. 8(b). Without too much alignment, we can achieve about 81% coupling of the TEM_{00} mode. There are also a small amount of TEM_{01} and TEM_{02} modes, which are induced by astigmatism and waist mismatch. The TEM_{03} mode is induced by the residual asymmetry. These results accord well with the numerical simulation shown in Fig. 5.

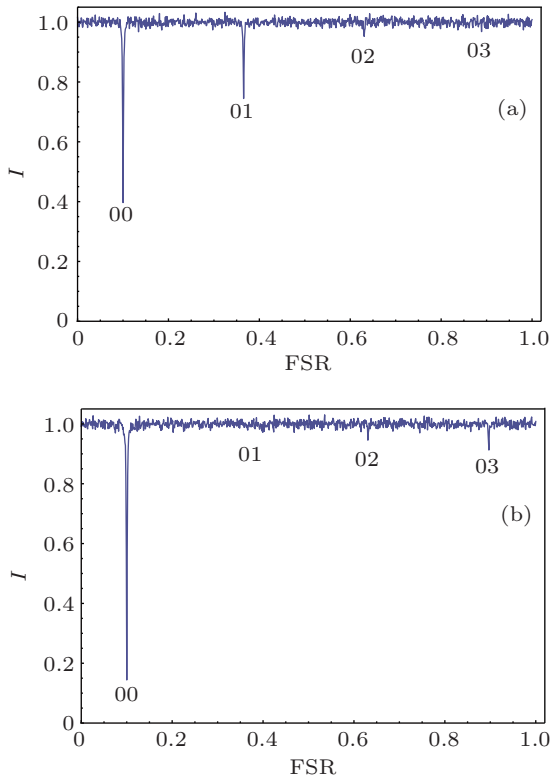


Fig. 8. (color online) Transmission spectrum of the distorted second harmonic generated by (a) a single bulk crystal and (b) walk-off compensating crystals when the mode cleaner is scanned.

To extract the TEM_{00} mode, we lock the cavity to the main transmission peak with PDH locking. Since there is still a residual phase modulation signal in the second harmonic, no extra EOM is required. The M^2 factor of the output from the mode cleaner is measured to be less than 1.001. The purified beam is then focused to the plane of the CCD camera with proper lenses, then it has a uniform phase distribution on this plane and can be an ideal phase reference.

To analyze the phase distribution of the distorted beam, we use the phase reference to interfere with it and scan the relative phase between them by exerting a ramp signal on the piezo mirror M4. By fitting the intensity variation trace at a point on the wavefront with a sinusoidal function, we can obtain the phase at this point. Since there is no walk off along the x axis, the generated beam should remain Gaussian in this direction. Thus we are only interested in the y axis. In this direction the intensity and phase distribution of the distorted second harmonic is reconstructed. Since the phase reconstruction is quite sensitive to the intensity at the spot of interest, we only focus on the area around the center of the beam. Outside this area the results are too noisy, so they are discarded. The results are shown in Fig. 9(a). We can see that the phase distribution of the beam is obviously asymmetric with its center, which is qualitatively in accordance with the numerical simulation results shown in Fig. 2. We also analyzed the phase distribution of the second harmonic generated at the present of two compensating crystals. The results are shown in Fig. 9(b). We can see that the asymmetry of the phase distribution becomes much more subtle than that generated by a single bulk crystal, as predicted in Fig. 4.

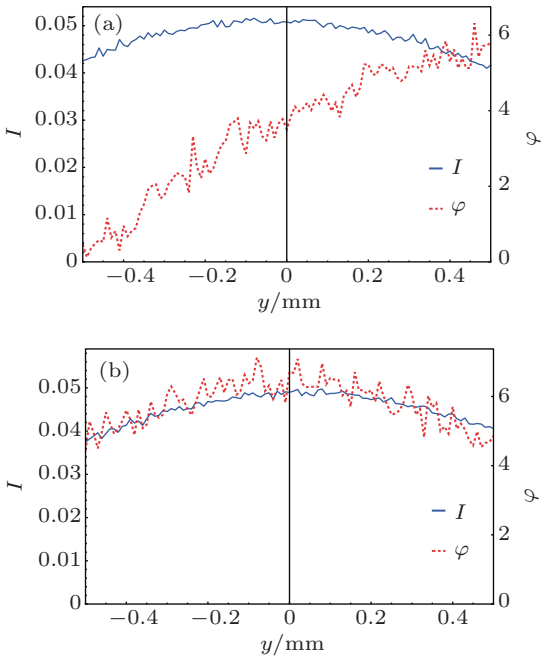


Fig. 9. (color online) Measured intensity (solid line) and reconstructed phase distributions (dashed line) of the distorted second harmonic generated by (a) a single bulk crystal (red line) and (b) two compensating crystals (blue line). All these distributions are along the y axis.

It should be noticed that the walk-off compensating configuration also helps to enhance the power of the generated second harmonic.[13] With the experimental parameters, the output power from the walk-off compensating crystals should be 1.3 times higher than that from a single bulk crystal, provided that the circulating power of the fundamental beam remains unchanged. However, in our experiment, the walk-off compensating crystals are not perfectly contacted due to our technique limitation. It will then induce additional loss at the interface and thus degrade the cavity finesse and impedance matching, which will lead to a decrease of the circulating power of the fundamental as well as the power of the generated second harmonic. In the experiment, we find that these two factors roughly cancel each other, and the output power of the second harmonic almost remains unchanged. It can be further improved if the two crystals are better contacted with

each other. Nevertheless, the suppression of the wavefront distortion by the walk-off compensating crystals still helps to extract more TEM_{00} mode component.

4. Conclusion

In conclusion, we analyzed the wavefront distortion of the second harmonic from a critically phase-matched SHG both theoretically and experimentally. The results show that the walk-off effect severely degrades the quality of the wavefront so that it can hardly be mode matched. To solve this problem, we adopted a distortion correction scheme using walk-off compensating crystals. According to numerical simulations, the performance of the scheme is tested to be excellent. The mechanism of the scheme is thoroughly analyzed, which can be a useful guide to the design of the compensating crystal configuration. In addition, we have made an experimental demonstration of this scheme, which is shown to be capable of suppressing the beam distortion significantly. Then with a mode cleaner we can extract the TEM_{00} mode with the efficiency of over 80%. Using this method, we can efficiently generate the second harmonic that is suitable for continuous-variable applications, even in the presence of the walk-off effect.

References

[1] Eimerl D 1987 *J. Quantum Electron.* **23** 1361
[2] Oka M, Liu L Y, Wiechmann W, Eguchi N and Kubota S 1995 *J. Sel. Top. Quantum Electron.* **1** 859
[3] Sasaki T, Mori Y and Yoshimura M 2003 *Opt. Mater.* **23** 343
[4] Scholz M, Opalevs D, Leisching P, Kaenders W, Wang G, Wang X, Li R and Chen C 2013 *Appl. Phys. Lett.* **103** 051114
[5] Steinbach A, Rauner M, Cruze F C and Bergquist J C 1996 *Opt. Commum.* **123** 207
[6] Zondy J J, Abed M and Khodja S 1994 *J. Opt. Soc. Am. B* **11** 2368
[7] Armstrong D J, Alford W J, Raymond T D, Smith A V and Bowers M S 1997 *J. Opt. Soc. Am. B* **14** 460
[8] Droz C, Kouta H and Kuwano Y 1999 *Opt. Rev.* **6** 97
[9] Zheng H, Zhang Y, Nie Z, Li C, Song J, Li C and Lu K 2009 *Chin. Phys. B* **18** 2729
[10] Qi B, Zhu W, Qian L and Lo H K 2010 *New J. Phys.* **12** 103042
[11] Chen Y, Shen Y, Tang G and Zou H 2013 *Chin. Phys. Lett.* **30** 110302
[12] Boyd G D and Kleinman D A 1968 *J. Appl. Phys.* **39** 3597
[13] Zondy J J, Bonnin C and Lupinski D 2003 *J. Opt. Soc. Am. B* **20** 1675
[14] Chen G, Shen Y, Liu Q and Zou H 2014 *Acta. Phys. Sin.* **63** 054204 (in Chinese)
[15] Zou H, Yue W, Chen G, Shen Y and Liu Q 2015 *Chin. Phys. Lett.* **32** 054207